Extensions to the generalized method of slices for stability analysis

Zu-Yu Chen

Water Conservancy and Hydroelectric Power Scientific Research Institute, P.O. Box 366, Beijing,
People's Republic of China

AND

N. R. Morgenstern

Department of Civil Engineering, University of Alberta, Edmonton, Alta., Canada T6G 2G7

Extensions are suggested to the generalized method of slices that is commonly used in slope stability analysis. It is shown that restrictions exist on the assumptions used to make the problem statically determinate. In addition, a numerical procedure has been developed to find the bounds to the factor of safety, subject to additional requirements of physical admissibility. As a result of these developments it has been possible to produce a revised computer program that appears to overcome the problems of convergence experienced by other programs in current use. Results obtained with this new analysis confirm the reliability of several methods of analysis used in practice.

On propose des développements à la méthode des tranches généralisée qui est couramment utilisée dans l'analyse de stabilité de pentes. On montre qu'il existe des restrictions aux hypothèses utilisées pour rendre le problème statiquement déterminé. De plus, une procédure numérique a été développée pour trouver les limites du facteur de sécurité compte tenu d'exigences supplé-mentaires d'admissibilité physique. Suite à ces développements il a été possible d'établir un programme d'ordinateur qui semble éliminer les problèmes de convergence rencontrés dans d'autres programmes actuellement en usage. Les résultats obtenus avec cette nouvelle analyse confirme la fiabilité de plusieurs méthodes de stabilité utilisées en pratique.

[Traduit par la revue]

Introduction

Generalized methods of slices are commonly used to investigate the stability of slopes, particularly when the section is nonhomogeneous. However, the problem is statically indeterminate and assumptions are necessary in order to obtain numerical results. Several methods have been advocated. For example, Janbu (1954, 1973) made assumptions regarding the location of the point of action of the interslice force and Morgenstern and Price (1965) and Spencer (1967, 1973) assumed the shape of the distribution of the inclination of the interslice force. Sarma (1973) adopted the distribution of the vertical component of the interslice forces.

A survey of the commonly used methods indicates the following.

1. The assumptions made for the different unknown variables involved in the equilibrium equations do not result in much difference in the final factor of safety. This is not surprising when considering that the various methods are based on the same equilibrium equations and the unknown variables are interrelated.

2. The assumptions regarding any unknown variable are not unique. A number of functions which lead to a group of solutions satisfying the equilibrium equations may be assumed. Some of the solutions should be rejected due to the requirement for physical admissibility (Morgenstern and Price 1965; Whitman and Bailey 1967; Janbu 1973). Since only the shape of the distribution of one of the unknown functions is assumed, the physical reasonableness cannot be checked until the final solution has been found. The selection of the assumed function depends to a large extent on intuition and experience but may be guided by stress analysis. Since we are basically confronted with an infinite number of possible choices for the assumed function, after performing several calculations we are still uncertain if some relevant solutions are missing or not.

The purpose of this paper is to overcome the disadvantages involved in the currently used methods by the following.

1. It will be shown that restrictions that have been ignored so far exist on the boundary values of the distributive assumption. The search for the solution to the equilibrium equations is then undertaken with a group of assumed functions that are fixed at both ends.

2. A method of sensitivity analysis to explore the influence of the assumed functions associated with physically reasonable solutions to the equilibrium equations will be developed. An efficient computer program for this method has been coded.

With the help of these two extensions, the bounds on the factor of safety caused by conditions of physical admissibility can be found. The effort required of the user is reduced considerably.

The general equilibrium equations

Limit equilibrium considerations in slope stability analysis are based on the following.

1. Principle of equilibrium

The sliding mass is divided into a number of slices. The requirements for force and moment equilibrium should be fully satisfied for every individual slice.

2. Mohr–Columb failure criterion

The Mohr–Columb failure criterion holds along the failure surface,

[1] $\tau = C' + \sigma_n' \tan \phi'$

where σ_n' = normal effective stress on the failure plane, τ = shear stress on the failure plane, C' = effective cohesion, and ϕ' = effective friction angle.

3. The factor of safety F

This is defined as that value by which the available shear strength parameters must be reduced in order to bring the soil mass into a state of limiting equilibrium along a given slip surface. Hence,

[2] $\tau = C_e' + (\tan \phi_e')\sigma_n'$

where

[3] $C_e' = C'/F$

[4] $\tan \phi_e' = (\tan \phi')/F$

and F = the factor of safety.

In addition to these considerations, there are conditions of physical admissibility (Morgenstern and Price 1965) as follows.

1. The shear force on the vertical surface of any slice should not exceed the shear strength that can be mobilized along the surface (Fig. 1),

[5] $F_v = [E' \tan \phi_{av}' + C_{av}'(y - z)]/X > F$

or

[6] $F_{ve} = F_v/F$

$= [E' \tan \phi_{ave}' + C_{ave}'(y - z)]/X > 1$

where F_v = factor of safety along the vertical surface of the slice, F_{ve} = relative factor of safety along the vertical surface of the slice, E' = effective normal force on the vertical surface, X = shear force on the vertical surface, $\tan \phi_{av}'$, C_{av}' = the average effective strength parameter on the vertical surface, $\tan \phi_{ave}'$, C_{ave}' = $\tan \phi_{av}'$, C_{av}' divided by the factor of safety, y = the ordinate of the slip surface, and z = the ordinate of the slope surface.

2. To avoid tensile stresses the line of action of the resultant effective normal force should not lie outside the vertical surface of the slice, i.e. (Fig. 2a),

[7] $0 < A_c' < 1$
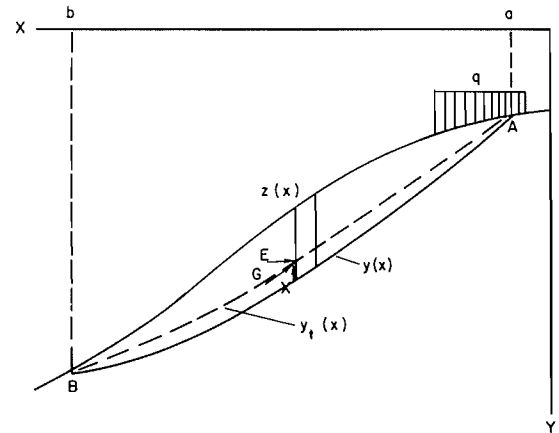

FIG. 1. The generalized failure surface.

where

[8] $A_c' = (y - y_t')/(y - z)$

and y_t' = the ordinate of the point of action of the effective normal force.

The general equilibrium equations for a slice can be expressed as

[9] $\cos(\phi_e' - \alpha + \beta)\dfrac{dG}{dx} - \sin(\phi_e' - \alpha + \beta)\dfrac{d\beta}{dx}G$

$= -\left[\dfrac{dW}{dx}\sin(\phi_e' - \alpha) + q \sin(\phi_e' - \alpha)\right.$

$\left. - r_u \dfrac{dW}{dx} \sec\alpha \sin\phi_e' + C_e' \sec\alpha \cos\phi_e'\right]$

[10] $G\sin\beta = -y\dfrac{d}{dx}(G\cos\beta) + \dfrac{d}{dx}(y_t G\cos\beta)$

where G = the resultant total force on the vertical side of the slice, β = the inclination of G to the horizontal, dW/dx = the weight of the slice per unit width, r_u = pore pressure ratio (Bishop and Morgenstern 1960), and q = vertical surface load.

Equation [9] can be obtained by substituting

[11] $E = G\cos\beta$

[12] $X = G\sin\beta$

into the equation of force equilibrium (eq. [10]) of Morgenstern and Price's paper (1965). However, the signs of the various terms of the two equations are not identical due to the different positive direction of the coordinate systems that have been used. Equation [9] can also be established by projecting all the forces acting on the slice to the axis A–A which is inclined at an angle of $(\phi' - \alpha)$ to the horizontal (Fig. 2b). In this case the resultant of N and S, the force P, which is inclined at an

angle of ϕ_e' to the normal, contributes nothing to the force equilibrium equation.

Equation [10] is obtained by considering the moment equilibrium about the midpoint of the base of the slice.

[13] $(G + \Delta G) \cos (\beta + \Delta\beta)[(y + \Delta y)$

$- (y_t + \Delta y_t) - \frac{1}{2}\Delta y]$

$- G \cos \beta (y - y_t + \frac{1}{2}\Delta y) + G (\sin \beta)\Delta x = 0$

Neglecting the small magnitudes of order higher than ΔG and $\Delta\beta$, [13] reduces to [10].

The corresponding boundary conditions are:

[14] $G(a) = 0$

[15] $G(b) = 0$

[16] $y_t(a) = y(a)$

[17] $y_t(b) = y(b)$

where a, b are abscissa values of the ends of the sliding mass.

If the slip surface terminates at a slope surface that is not vertical, the slices at both ends are triangles rather than rectangles. It is then required that the value of β and A_c be fixed at points A and B. A detailed discussion will be given in a subsequent section.

By virtue of [14]–[17], [10] can be integrated:

[18] $\displaystyle\int_a^b G(\sin \beta - \tan \alpha \cos \beta) \, dx = 0$

For brevity, [9] is rewritten as

[19] $\dfrac{dG}{dx} - \tan \psi_e' \dfrac{d\beta}{dx} G = -p(x) \sec \psi_e'$

where

(a)

(b)

FIG. 2. The force equilibrium of a slice.

[20] $p(x) = \dfrac{dW}{dx} \sin (\phi_e' - \alpha) + q \sin (\phi_e' - \alpha) - r_u \dfrac{dW}{dx} \sec \alpha \sin \phi_e' + C_e' \sec \alpha \cos \phi_e'$

[21] $\psi_e' = \phi_e' - \alpha + \beta$

By substituting the boundary condition of [14], the solution to [19] is

[22] $G(x) = - \exp \left[\left[\displaystyle\int_a^x \tan (\phi_e' - \alpha + \beta) \dfrac{d\beta}{d\zeta} \, d\zeta \right] \int_a^x p(\xi) \sec \psi_e' \exp \left[- \int_a^\xi \tan (\phi_e' - \alpha + \beta) \dfrac{d\beta}{d\zeta} \, d\zeta \right] d\xi \right.$

where ξ and ζ are dummy variables substituting for x.

Substitution of [15] into [22] yields

[23] $\displaystyle\int_a^b p(x)s(x) \, dx = 0$

where

[24] $s(x) = \sec \psi_e' \exp \left[- \displaystyle\int_a^x \tan \psi_e' \dfrac{d\beta}{d\zeta} \, d\zeta \right]$
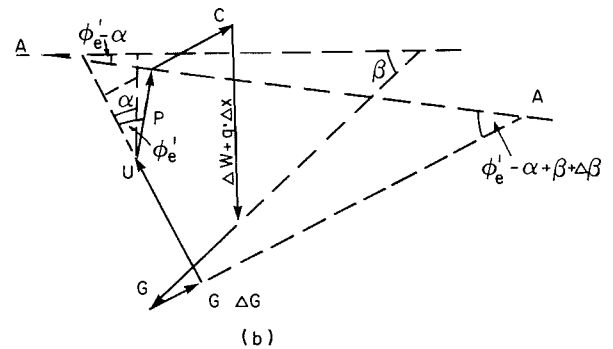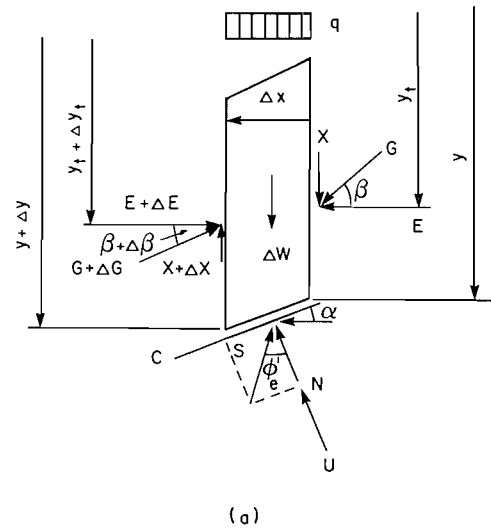
Substituting [22] into [18] and integrating by parts, we obtain

$$[25] \quad \int_a^b p(x)s(x)t(x)\,\mathrm{d}x = 0$$

where

$$[26] \quad t(x) = \int_a^x (\sin\beta - \cos\beta\tan\alpha)\exp\left[\int_a^\xi \tan(\phi_e' - \alpha + \beta)\frac{\mathrm{d}\beta}{\mathrm{d}\zeta}\,\mathrm{d}\zeta\right]\mathrm{d}\xi$$

Equations [23] and [25] are governing equations for the calculation of the factor of safety.

The function $p(x)$, which does not contain $\beta(x)$, accounts for the geometrical and physical properties of the slope. The function $s(x)$ takes into account the assumption that will be made for $\beta(x)$. For an assumed function $\beta(x)$, the value of F that satisfies [23] and [25] may be found. It has been shown (Chen 1981) that [23] and [25] are reducible to special cases, such as the wedge slide analysis, Bishop's simplified method (Bishop 1955), the logarithmic spiral method (Taylor 1948), and Spencer's method (Spencer 1967) if the appropriate simplifying conditions are considered.

Boundary values for $\beta(x)$ and A_c

As noted previously, in order to render the problem statically determinate, an assumption about the side force can be made. Morgenstern and Price (1965) assumed that

$$[27] \quad \tan\beta = \lambda f(x)$$

where $f(x)$ is an assumed function and λ is a coefficient to be determined.

Janbu (1973) assumed that

$$[28] \quad A_c = \tfrac{2}{3}$$

where

$$[29] \quad A_c = (y - y_t)/(y - z)$$

and y_t = the ordinate of the point of action of the total normal force.

Basically, A_c and $\lambda f(x)$ could be any function. However, the values of A_c and $\lambda f(x)$ at the boundary points A and B should be fully specified if the slip surface terminates at a surface slope that is not vertical. This marks a distinction from the previously published work.

Point A is a special point where the ratio of X to E is equal to the ratio of τ_{xy} to σ_x, i.e. (see Fig. 3),

$$[30] \quad \tan\beta_a = \lim_{x\to a}\frac{X}{E} = \frac{\tau_{xy}}{\sigma_x}$$

where β_a = the inclination of the total side force G at the boundary point A, and τ_{xy}, σ_x = the shear and normal

stress on CB, the vertical side of the end element ACB.

If the stress tensor at point A is determined, β will be fixed as well.

The stresses can be determined by drawing the Mohr circle as shown in Fig. 3, in which the general case of the end slice ABC with a sloping surface AB and a vertical load q is considered. Point A in the Mohr circle represents the stress state along the surface AB of the element. Since

$$[31] \quad \sigma_s = q\cos^2\gamma$$

$$[32] \quad \tau_s = q\sin\gamma\cos\gamma$$

the angle AOC in the Mohr circle (Fig. 3b) is equal to γ.

It is required that the Mohr circle in Fig. 3b pass through point A, be tangent to the Mohr–Coulomb failure line GD, and make the angle ABD equal to $\alpha - \gamma$. The circle is therefore unique. The stress state on any plane of the element is represented by a point on the Mohr circle that is the intersection point of the Mohr circle and a straight line passing through point B and parallel to the plane concerned, provided the X axis of the Mohr circle is parallel to the direction of the minor principal stress of the element. For example, the stress state of the failure surface AC in Fig. 3a is represented by the point D in the Mohr circle that makes BD inclined at an angle of $\alpha - \gamma$ to AB.

Consider point E in Fig. 3b, which makes the angle EOC equal to γ (E is on the minus side of the Mohr circle). Point E represents the stress state of a surface in the element on which

$$[33] \quad \tau_{xy}/\sigma_x = -\tan\gamma$$

In Fig. 3b, it can be shown that EB is inclined at an angle of $90° - \gamma$ to AB. This indicates that the surface represented by point E in the Mohr circle is the one in the element that is inclined at an angle $(90° - \gamma)$ to the surface AB. This plane is nothing else but the vertical surface BC of the element. Hence the stress state on the vertical surface should satisfy [33]. In other words, the side force on the vertical surface BC of the end slice should be parallel to the surface slope AB of the slice if the width of the slice is sufficiently small.

The need for determining the boundary values for $\beta(x)$ is actually based on the requirement for satisfying
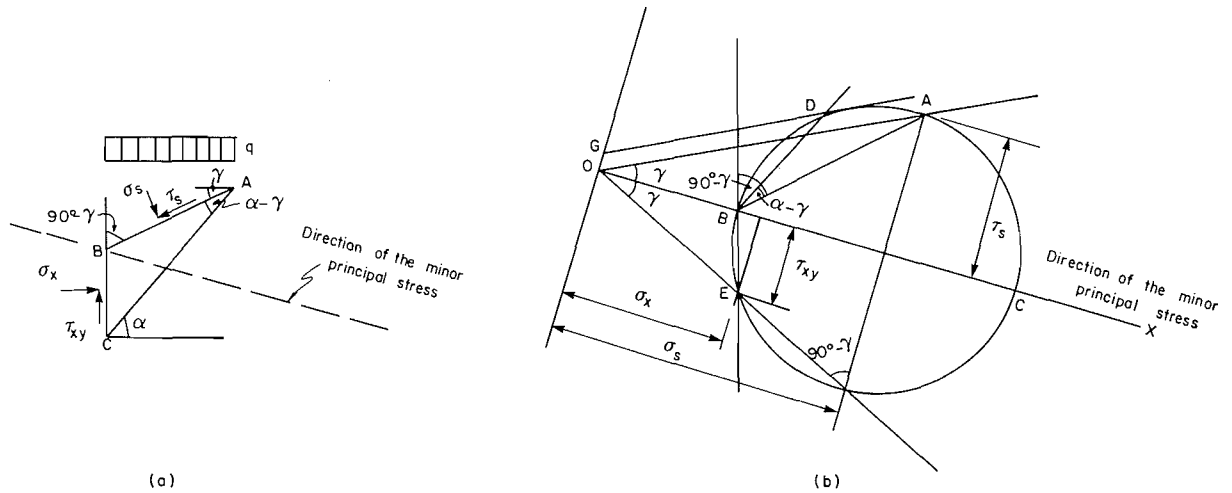
FIG. 3. The determination of the inclination of the end slice. Diagram of: (a) the end slice; (b) the Mohr circle of the end slice.

the moment equilibrium. For the end slices at A and B, since the values of G and $y - y_t$ are equal to zero, all terms of first-order magnitude in [13] are zero. The second-order small magnitudes can no longer be neglected as was done for normal slices during the derivation of the moment equilibrium in [10]. The consideration of second-order magnitudes in [13] will lead to the principle of complementary shear stresses that eventually determines the boundary values of β. In other words, if the values of β are taken arbitrarily at A and B, the solution will correspond to one in which the principle of complementary shear stresses does not hold. The value of A_c at points A can also be determined due to the fact that CB (Fig. 3a), the area over which the force E is applied, is infinitesimally small. The restrictions that fix the boundary values of β and A_c are presented here; formal demonstrations are contained in detailed work available from the authors.

Restriction 1

The resultant total force acting on the vertical side of the end slice is parallel to the surface of the slope if the width of the end slice is sufficiently small, i.e.,

[34] $\beta_a = \gamma_a$

where γ_a and β_a are the inclination of the slope surface and side force G, respectively, at points A.

Restriction 2

The point of action of the total normal force on the vertical side of the end slice is located at the midpoint in case A and the lower one-third point in case B if the width of the slice is sufficiently small, i.e., $A_c = \frac{1}{2}$ for case A and $A_c = \frac{2}{3}$ for case B, where case A and case B are defined as the following.

Case A

At the end points A or B, the soil is cohesive or there

is some vertical surcharge on the slope surface, i.e., $C(a) \neq 0$ or $q(a) \neq 0$.

Case B

At the end points A and B, (1) the soil is cohesionless, i.e., $C(a) = 0$; (2) there is no surcharge on the slope surface, i.e., $q(a) = 0$; and (3) the slip surface is not tangent to the slope

$$y'(a) - z'(a) \neq 0$$

or

$$\left. \frac{d^2 W}{dx^2} \right|_{x=a} \neq 0$$

where $y'(a), z'(a)$ are the derivatives of $y(x)$ and $z(x)$ with respect to x at point A.

The numerical procedure

By linearizing the value of $\alpha(x)$ and some other variables for each slice, Morgenstern and Price (1967) developed a numerical procedure based on the Newton–Raphson method for solving differential equations. This method has been refined in the following aspects to satisfy the required boundary conditions and to make the iteration more effective.

As mentioned before, the boundary values of the side force function $\beta(x)$ should be fixed. This can be done by taking tan β as

[35] $\tan \beta = \lambda f(x) + f_0(x)$

where $f(x)$ is the assumed function, which is equal to zero at both ends, λ is a coefficient to be determined, and $f_0(x)$ is another function that has the required values at both ends, i.e.,

[36] $f(a) = 0$

[37] $\quad f(b) = 0$

[38] $\quad f_0(a) = \tan \beta_a$

[39] $\quad f_0(b) = \tan \beta_b$

Basically, $f(x)$ and $f_0(x)$ can be arbitrary functions; however, in some cases, an inappropriate selection of $f(x)$ and $f_0(x)$ will cause difficulties in the iteration procedure, as will be discussed subsequently.

The iteration procedure starts by substituting assumed values (λ_1 and F_1) into [23] and [25]. If λ_1 and F_1 make the values of

[40] $\quad G_n = G(\lambda_1, F_1) = \displaystyle\int_a^b p(x, \lambda_1, F_1) s(x, \lambda_1, F_1)\, dx$

[41] $\quad M_n = M(\lambda_1, F_1) = \displaystyle\int_a^b p(x, \lambda_1, F_1) s(x, \lambda_1, F_1)$
$$\times\, t(x, \lambda_1, F_1)\, dx$$

not close to zero within the tolerable limit, the next iterative values $\lambda_1 + \Delta\lambda$ and $F_1 + \Delta F$ that are supposed to make G_n and M_n close to zero were given by (Morgenstern and Price 1967) as

[42] $\quad \Delta\lambda = \left.\dfrac{-G_n \dfrac{\partial M_n}{\partial F} + M_n \dfrac{\partial G_n}{\partial F}}{\dfrac{\partial G_n}{\partial \lambda}\dfrac{\partial M_n}{\partial F} - \dfrac{\partial G_n}{\partial F}\dfrac{\partial M_n}{\partial \lambda}}\right|_{\lambda=\lambda_1, F=F_1}$

[43] $\quad \Delta F = \left.\dfrac{G_n \dfrac{\partial M_n}{\partial \lambda} - M_n \dfrac{\partial G_n}{\partial \lambda}}{\dfrac{\partial G_n}{\partial \lambda}\dfrac{\partial M_n}{\partial F} - \dfrac{\partial G_n}{\partial F}\dfrac{\partial M_n}{\partial \lambda}}\right|_{\lambda=\lambda_1, F=F_1}$

Instead of calculating $\partial M_n/\partial F$, $\partial G_n/\partial F$, $\partial M_n/\partial \lambda$, $\partial G_n/\partial \lambda$ by linearization of the function $\alpha(x)$, we proceed here analytically:

[44] $\quad \dfrac{\partial G_n}{\partial F} = \displaystyle\int_a^b p(x)s(x)\left[k(x) - \int_a^x \sec^2 \psi_e' \dfrac{d\phi_e'}{dF}\dfrac{d\beta}{d\xi}\, d\xi \right] dx$

[45] $\quad \dfrac{\partial M_n}{\partial F} = \displaystyle\int_a^b p(x)s(x)\left[k(x)t(x) - \int_a^x t\sec^2 \psi_e' \dfrac{d\phi_e'}{dF}\dfrac{d\beta}{d\xi}\, d\xi \right] dx$

[46] $\quad \dfrac{\partial G_n}{\partial \lambda} = \displaystyle\int_a^b p(x)s(x)\left[-\int_a^x \sec^2 \psi_e' \dfrac{d\beta}{d\lambda}\dfrac{d\alpha}{d\xi}\, d\xi + D_i \right] dx$

[47] $\quad \dfrac{\partial M_n}{\partial \lambda} = \displaystyle\int_a^b p(x)s(x)\left[-\int_a^x t\sec^2 \psi_e' \dfrac{d\beta}{d\lambda}\dfrac{d\alpha}{d\xi}\, d\xi + D_{ti} \right.$
$$\left. +\int_a^x \cos \phi_e' \sec \alpha \sec \psi_e' \exp\left\{ \int_a^\xi \tan \psi_e' \dfrac{d\beta}{d\zeta}\, d\zeta \right\} \dfrac{d\beta}{d\lambda}\, d\xi \right] dx$$

where

[48] $\quad k(x) = -\left[\left(\dfrac{dW}{dx} + q\right)\sin \phi_e' \cos \beta - r_u \dfrac{dW}{dx}\sec \alpha \cos(\beta - \alpha)\sin \phi_e' + C_e' \sec \alpha \cos \phi_e' \cos(\beta - \alpha) \right]$
$$\times \cos \phi_e' \bigg/ \left\{ F\left[\left(\dfrac{dW}{dx} + q\right)\sin(\phi_e' - \alpha) - r_u \dfrac{dW}{dx}\sec \alpha \sin \phi_e' + C_e' \sec \alpha \cos \phi_e' \right]\cos(\phi_e' - \alpha + \beta) \right\}$$

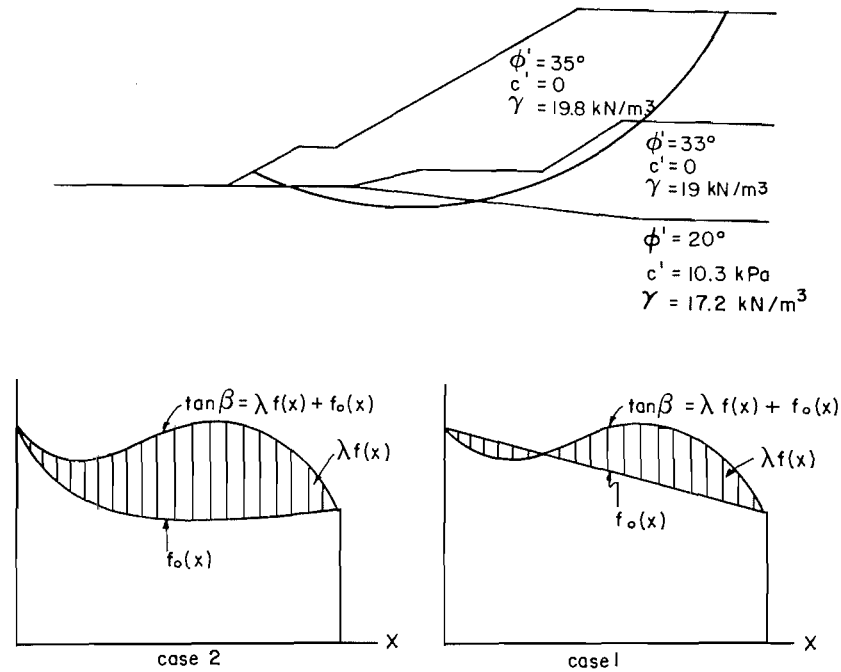[49] $\quad \dfrac{d\beta}{d\lambda} = (\cos^2 \beta)f(x)$

[50] $\quad D_i = \left.\tan \psi_a' \dfrac{d\beta}{d\lambda}\right|_{x=a} - \displaystyle\sum_{i=1}^{s}\left[\tan \psi_{ei}' \dfrac{d\beta_i}{d\lambda} \right]_l^r$

[51] $\quad D_{ti} = -\displaystyle\sum_{i=1}^{s}\left[t_i \tan \psi_{ei}' \dfrac{d\beta_i}{d\lambda} \right]_l^r$

where D_i, D_{ti} are coefficients accounting for the possible discontinuity of ϕ_e' or α at certain point i at which the value of ϕ_e' or α changes abruptly from $[\phi_{ei}']_r$, $[\alpha_i]_r$ to $[\phi_{ei}']_l$, $[\alpha_i]_l$; the superscript r and subscript l represent the values at the right and left side at this point of discontinuity.

The derivation of [44]–[47] may also be found in detailed work available from the authors.

$$\phi' = 35°$$
$$c' = 0$$
$$\gamma = 19.8 \text{ kN/m}^3$$

$$\phi' = 33°$$
$$c' = 0$$
$$\gamma = 19 \text{ kN/m3}$$

$$\phi' = 20°$$
$$c' = 10.3 \text{ kPa}$$
$$\gamma = 17.2 \text{ kN/m}^3$$

The process of iteration

case 1		case 2	
F	λ	F	λ
2.030	0.010	2.030	0.010
2.068	-0.090	2.038	0.733
2.058	0.115	2.051	0.673
2.065	-0.036	2.051	0.669
1.947	2.481		
2.051	1.358		
2.049	0.461		
2.057	0.163		
2.063	0.002		
2.079	-0.334		
2.069	-0.165		
2.064	-0.022		
2.107	-0.925		
1.995	-0.617		
2.059	-0.408		
2.068	-0.209		
2.065	-0.062		
2.048	0.327		
2.058	0.108		
...	...		

FIG. 4. An example showing the selection of $f(x)$ and $f_0(x)$.

Since the condition of fixing the boundary value by [38] and [39] is not used in the derivation of [44]–[47], the latter are applicable to cases where the boundary values of $\beta(x)$ are not fixed. If it is not desired to fix the boundary value of $\beta(x)$, for example, when the case of $f(x) = 1$ of the Morgenstern–Price method is evaluated, then it is simple to take $f(x) = 1$ and $f_0(x) = 0$. Equations [44]–[47] still apply.

The problem of convergence is a common concern during the iteration. The refinement for the computation of the derivatives described previously, in combination with the following techniques, facilitates convergence.

(1) The assumed function $f(x)$ is selected to have the same sign throughout the region (a, b). Figure 4 shows an example in which two different choices of $f(x)$ and $f_0(x)$ consistent with the same $\tan \beta$ are used. In case 2, the value of $\tan \beta$ will increase or decrease as a whole with an increment of λ, while in case 1 only part of the value of $\tan \beta$ will be increased and the rest will be decreased. As a result, G_n and M_n may not be monotonic in λ and some difficulties may be experienced in iteration. The table in Fig. 4 shows that case 2 successfully converges but case 1 fails to converge.

(2) The assumed values of F_1 and λ_1 are estimated as closely as possible to the final solution. Some of the simplified methods such as that of Fellenius could be

used for the estimation of the factor of safety. Chen (1981) suggested a simplified equation that is applicable to generalized failure surfaces and gives reasonable estimates without the need of iteration.

For estimating the value of λ_1, it is suggested that the average value of $\beta(x)$ be taken as equal to the average inclination of the slip surface, i.e.,

$$[52] \quad \int_a^b \tan \beta \, dx = \int_a^b \tan \alpha \, dx$$

By substituting [35] into [52], it is easy to find the value of λ_1 for the first iteration.

Another way of estimating the values of F_1 and λ_1 is to estimate a number of sets of F_1 and λ_1 that possibly cover the accurate values and substitute them into [42] and [43]. The accurate values of F and λ, which make G_n and M_n in [42] and [43] equal to zero, will in turn result in zero values of ΔF and $\Delta \lambda$. The set of F_1 and λ_1 that gives the minimum value of $\Delta \lambda^2 + \Delta F^2$ is therefore very likely close to the accurate value of F and λ and makes the problem converge effectively.

With the refinements described in this section, the numerical procedure has converged in every case investigated.

Upper and lower bound solutions for factor of safety

By assuming different side force functions, a number of solutions for the factor of safety can be found. However, the physically acceptable solutions are limited within reasonably narrow bounds. In order to find the bound, it is advantageous to investigate how the value of F changes with a variation of side force function $\beta(x)$ that is required to be physically reasonable.

Suppose there is a set of solutions F^* and $\beta^*(x)$ that satisfies the force and moment equilibrium equations [23] and [25], i.e.,

$$[53] \quad G_n = \int_a^b p(F^*, \beta^*)s(F^*, \beta^*) \, dx = 0$$

$$[54] \quad M_n = \int_a^b p(F^*, \beta^*)s(F^*, \beta^*)t(F^*, \beta^*) \, dx = 0$$

If a neighbouring solution of $F^* + \Delta F$, $\beta^* + \Delta \beta$ also satisfies [23] and [25], we have

$$[55] \quad \Delta G_n = \int_a^b p(F^* + \Delta F, \beta^* + \Delta \beta)s(F^* + \Delta F, \beta^* + \Delta \beta) \, dx - \int_a^b p(F^*, \beta^*)s(F^*, \beta^*) \, dx = 0$$

$$[56] \quad \Delta M_n = \int_a^b p(F^* + \Delta F, \beta^* + \Delta \beta)s(F^* + \Delta F, \beta^* + \Delta \beta)t(F^* + \Delta F, \beta^* + \Delta \beta) \, dx$$
$$- \int_a^b p(F^*, \beta^*)s(F^*, \beta^*)t(F^*, \beta^*) \, dx = 0$$

Equations [55] and [56] indicate that the variation of G_n and M_n due to the increment of F^* and $\beta^*(x)$ should be zero if $F^* + \Delta F$ and $\beta^* + \Delta \beta$ is another set of solutions of [23] and [25].

Let $\Delta \beta(x)$ take the form

$$[57] \quad \Delta \beta = \varepsilon \eta(x)$$

where ε is a coefficient that makes $\Delta \beta$ sufficiently small in comparison to the corresponding values of β. It can be shown that

$$[58] \quad \Delta G_n = K_{gf}\Delta F + K_{ga}\varepsilon + o(\Delta F, \varepsilon)$$

$$[59] \quad \Delta M_n = K_{mf}\Delta F + K_{ma}\varepsilon + o(\Delta F, \varepsilon)$$

where

$$[60] \quad K_{gf} = \int_a^b p(x)s(x)\left[k(x) - \int_a^x \sec^2 \psi_e' \frac{d\phi_e'}{dF} \frac{d\beta}{d\xi} \, d\xi \right] dx$$

$$[61] \quad K_{mf} = \int_a^b p(x)s(x)\left[k(x)t(x) - \int_a^x t \sec^2 \psi_e' \frac{d\phi_e'}{dF} \frac{d\beta}{d\xi} \, d\xi \right] dx$$

$$[62] \quad K_{ga} = \int_a^b p(x)s(x)\left[-\int_a^x \sec^2 \psi_e' \frac{d\alpha}{d\xi}\eta(\xi) \, d\xi + B_i \right] dx$$

$$[63] \quad K_{ma} = \int_a^b p(x)s(x) \left[-\int_a^x t \sec^2 \psi_e' \frac{d\alpha}{d\xi} \eta(\xi) \, d\xi + B_{ti} \right.$$

$$\left. + \int_a^x \cos \phi_e' \sec \alpha \sec \psi_e' \exp \left\{ \int_a^\xi \tan \psi_e' \frac{d\beta}{d\zeta} \, d\zeta \right\} \eta(\xi) \, d\xi \right] dx$$

$$[64] \quad B_i = -\sum_{i=1}^s [\tan \psi_{ei}' \eta(x_i)]_l^r + \tan \psi_{ea}' \eta(a)$$

$$[65] \quad B_{ti} = -\sum_{i=1}^s [t_i \tan \psi_{ei}' \eta(x_i)]_l^r$$

and $o(\Delta F, \varepsilon)$ represents a small magnitude of order higher than ΔF and ε. The details of the derivation of [60]–[63] can also be obtained from the authors.

Substituting [58] and [59] into [55] and [56], and neglecting $o(\Delta F, \varepsilon)$, we have

$$[66] \quad K_{gf}(F^*, \beta^*)\Delta F + K_{ga}(F^*, \beta^*, \eta(x))\varepsilon = 0$$

$$[67] \quad K_{mf}(F^*, \beta^*)\Delta F + K_{ma}(F^*, \beta^*, \eta(x))\varepsilon = 0$$

Equations [66] and [67] have non-zero solutions for ΔF and ε only when

$$[68] \quad \begin{vmatrix} K_{gf}(F^*, \beta^*) & K_{ga}(F^*, \beta^*, \eta(x)) \\ K_{mf}(F^*, \beta^*) & K_{ma}(F^*, \beta^*, \eta(x)) \end{vmatrix} = 0$$

which indicates that if $F^* + \Delta F$ and $\beta^* + \varepsilon\eta(x)$ is a set of solutions of [23] and [25], $\eta(x)$ must be selected in such a way that [68] holds. Once the value of $\eta(x)$ satisfying [68] has been found, ΔF can be obtained by solving [66] or [67] with a specified value of ε that makes $\eta(x)$ sufficiently small. The smaller the value of ε is, the more accurate the new solution will be. After performing this procedure several times, it is possible to obtain a new solution that is distinct from the original solution and satisfies [23] and [25] with the required accuracy.

To find $\eta(x)$, let

$$[69] \quad \eta(x) = m\eta_1(x) + \eta_2(x)$$

where $\eta_1(x)$ and $\eta_2(x)$ are arbitrary functions that are linearly independent, namely,

$$[70] \quad \eta_2(x) \neq C_1\eta_1(x) + C_2$$

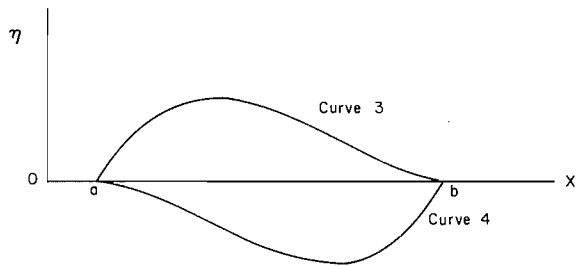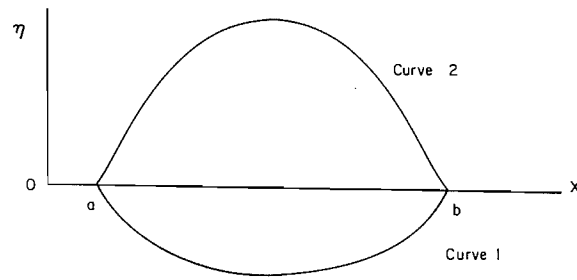where C_1 and C_2 are constants.

By substituting [69] into [68], we obtain

$$[71] \quad m = -\frac{K_{gf}(F^*, \beta^*)K_{ma}(F^*, \beta^*, \eta_2(x)) - K_{mf}(F^*, \beta^*)K_{ga}(F^*, \beta^*, \eta_2(x))}{K_{gf}(F^*, \beta^*)K_{ma}(F^*, \beta^*, \eta_1(x)) - K_{mf}(F^*, \beta^*)K_{ga}(F^*, \beta^*, \eta_1(x))}$$

Substitution of [69] into [66] yields

$$[72] \quad \Delta F = -\frac{K_{ga}(F^*, \beta^*, \eta(x))}{K_{gf}(F^*, \beta^*)} \varepsilon$$

and

$$[73] \quad \Delta\beta = \varepsilon\eta(x) = \varepsilon[m\eta_1(x) + \eta_2(x)]$$

Basically, $\eta_1(x)$ and $\eta_2(x)$ can be arbitrary functions. Attention should be paid to the case where $\beta^*(x)$ is zero at a certain point. In that case, in order to ensure that $\Delta\beta$ is smaller than $\beta^*(x)$, it is advantageous to specify that $\eta_1(x)$ and $\eta_2(x)$ are also equal to zero at that point.

For our purpose here, two sets of $\eta_1(x)$ and $\eta_2(x)$ may be used.

The first set of $\eta_1(x)$ and $\eta_2(x)$ is selected as an elliptic and a parabolic function (curves 1 and 2 in Fig. 5). The function $\eta(x)$ has positive values in the middle part of the region (a, b) and negative values of both sides if ε is positive and m is less than 2. This results in an increase of $\beta(x)$ in the middle part and a decrease on both sides. If ε is negative, $\beta(x)$ will be decreased in the middle part

and increased on both sides. Thus, the first set of $\eta_1(x)$ and $\eta_2(x)$ will result in an upward or downward movement of the peak value of $\beta(x)$.

The second set of $\eta_1(x)$ and $\eta_2(x)$ (curves 3 and 4 in Fig. 5) are selected as cubic polynomial functions with the peak values on the left and right sides respectively. The function $\beta(x)$ is positive on the left side and negative on the right side if ε is positive and m is near 1. This results in a movement of the peak values of $\beta(x)$ to the left. A negative value of ε will result in a movement of the peak value to the right.

Because the behaviour of F_{ve}, the factor of safety along the vertical surface of the slices, is related to $\beta(x)$, the movement of the peak value of $\beta(x)$ will eventually make F_{ve} reach the bound beyond which the value of F_{ve} is less than unity and the requirement of physical admissibility for F_{ve} is not satisfied. From the equation

$$[74] \quad y_t = y + \frac{\int_a^x G(\sin \beta - \cos \beta \tan \alpha) \, dx}{G \cos \beta}$$

η

Curve 2

0   a   b   X

Curve I

η

Curve 3

0   a   b   X

Curve 4

Curve I $\eta_1(x) = -\{1-(2(x-a)/(b-a)-1)^2\}^{0.5}$

Curve 2 $\eta_2(x) = -8(x-b)(x-a)/(b-a)^2$

Curve 3 $\eta_1(x) = 6.75(x-b)^2(x-a)/(b-a)^3$

Curve 4 $\eta_2(x) = 6.75(x-b)(x-a)^2/(b-a)^3$

$\eta(x) = \eta_2(x) + m\eta_1(x)$

$\Delta \beta(x) = \epsilon \ \eta(x)$

FIG. 5. The integration function $\eta(x)$.

it can be inferred that an increase of the average value of $\beta(x)$ in the region (a,x) will result in an increase of the value of y_t at x and in turn a decrease of A_c. Therefore, if $\eta_1(x)$ and $\eta_2(x)$ are selected as curves 3 and 4, the value of A_c' will probably decrease with a positive value of ϵ and increase with a negative value of ϵ.

In the examples that follow it will be shown how the value of A_c' or F_{ve} moves to the bound by an appropriate selection of the set of integration curves $\eta_1(x)$, $\eta_2(x)$ and the value of ϵ.

Illustrative examples

A computer program has been coded at the University of Alberta to undertake the calculation and a plotting program has also been added to assist in interpreting the computations.

Example 1

Find the factor of safety of the slope shown in Fig. 6 for the circular failure surface 1. Also find the factor of safety for circular failure surface 2 under drained conditions.

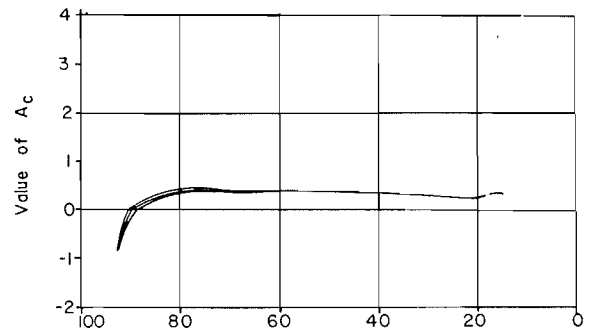| Soil	Unit Weight (kN/m³)	ϕ'	c' (kPa)	Cu (kPa)
1	20.10	38	0	10.06
2	19.63	23	5.27	19.64
3	17.27	20	7.19	26.35
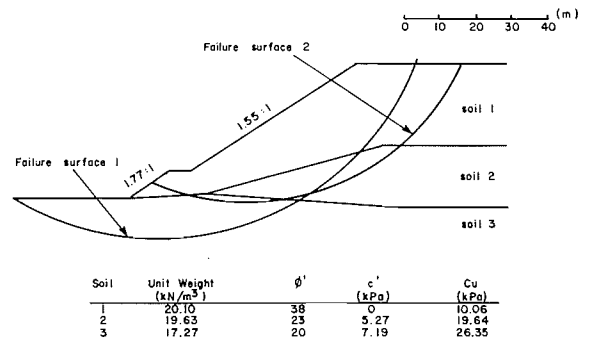
FIG. 6. Example 1.
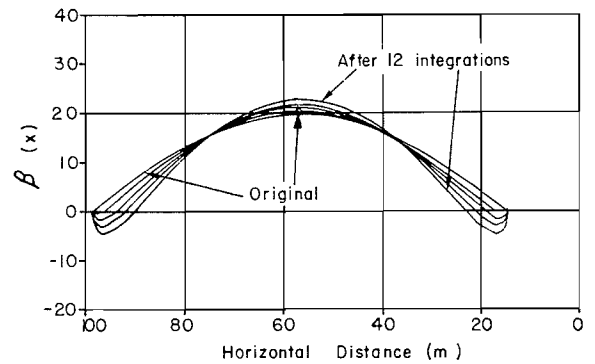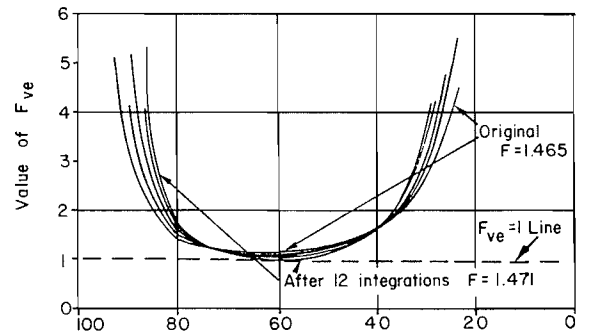
FIG. 7. The peak value of $\beta(x)$ moves upward (example 1). Curves 1 and 2 were employed; $\epsilon = 0.025$.
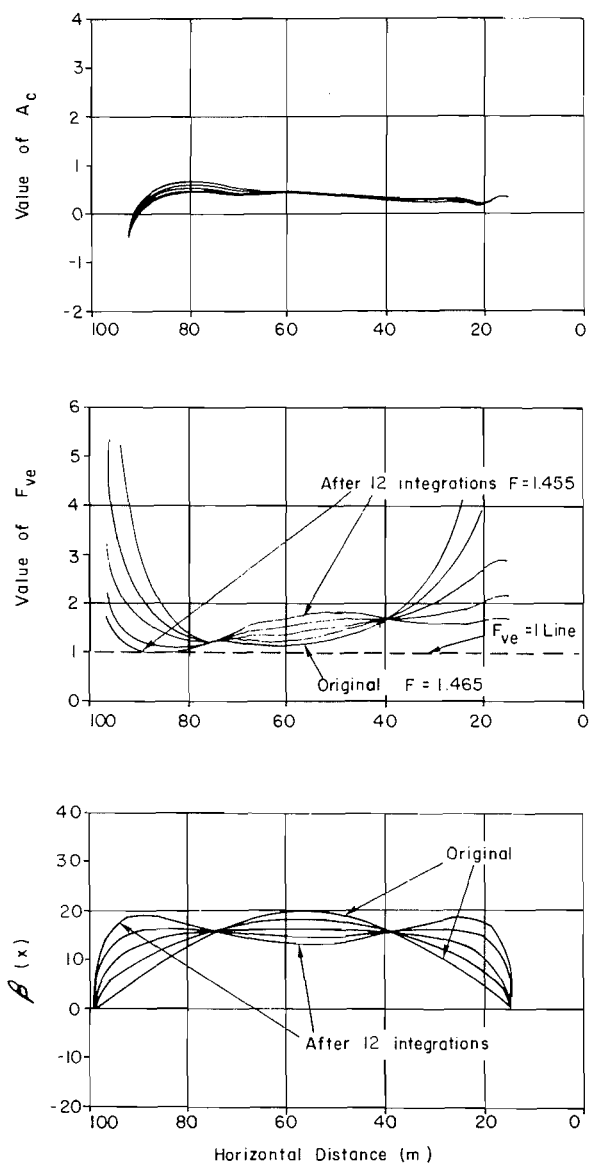
FIG. 8. The peak value of $\beta(x)$ moves downward (example 1). Curves 1 and 2 were employed; $\varepsilon = -0.025$.

Failure surface 1

The analysis using effective strength parameters was first performed. The failure surface terminates at the horizontal slope at both ends. A sine function is selected for $f(x)$, and $f_0(x)$ is taken as zero. The values of F and λ were found to be 1.465 and 0.360 respectively. The curves of F_{ve} and A_c' associated with the original case in Fig. 7 show that this is a physically reasonable solution. However, the value of F_{ve} approaches the $F_{ve} = 1$ line in the middle part of the region. If the value of $\beta(x)$ is increased in the middle part by employing curves 1 and 2
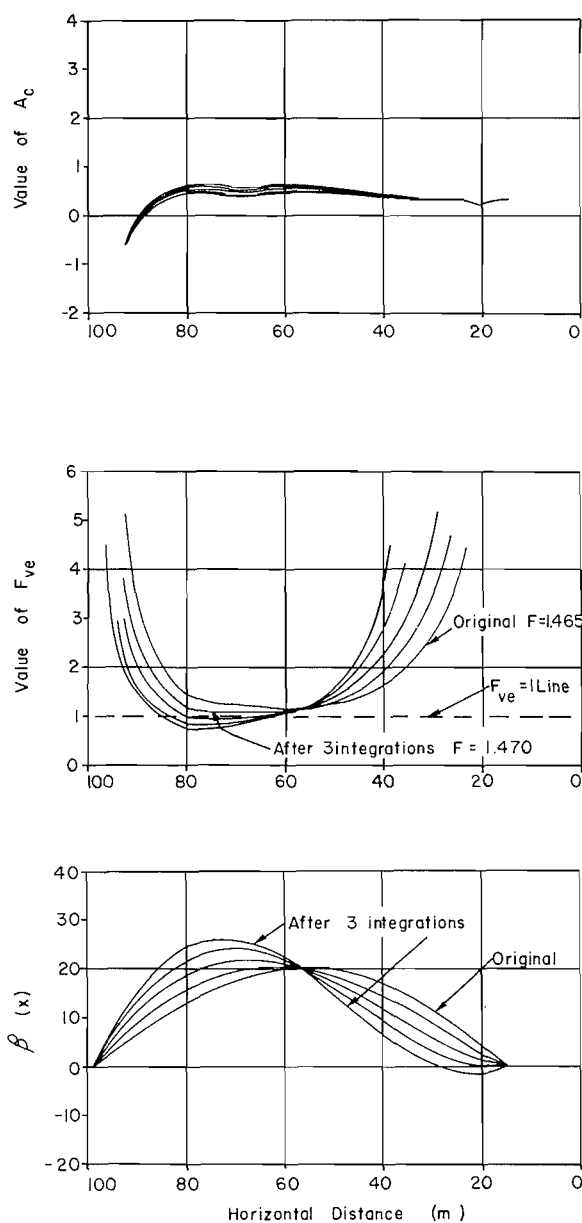
FIG. 9. The peak value of $\beta(x)$ moves to the left (example 1). Curves 3 and 4 were employed; $\varepsilon = -0.025$.

with a positive ε value of 0.025, the value of F_{ve} will eventually go below unity in the middle part. Figure 7 shows the progress of the integration. After 12 integrations, the lowest value of F_{ve} was less than unity; the integration in this direction was then stopped. The corresponding values of the factor of safety change from 1.465 to 1.471. An integration in the opposite direction can be made by taking ε as -0.05 as shown in Fig. 8. The value of F_{ve} increases in the middle part and

FIG. 10. The peak value of $\beta(x)$ moves to the right (example 1). Curves 3 and 4 were employed; $\varepsilon = 0.04$.

decreases on both sides. The F_{ve} curve eventually touches the $F_{ve} = 1$ line after 12 integrations. The factor of safety changes from 1.465 to 1.455.

Curves 3 and 4 are used to move the peak value of $\beta(x)$ to the right and left by taking ε equal to 0.04 and -0.025 respectively (Figs. 9 and 10). The values of the factor of safety associated with the solutions touching the $F_{ve} = 1$ line were 1.444 and 1.470 after nine and three integrations respectively.

Curve	Integration Function	Time of Integration	ϵ	F
1	Original			0.940
2	curve 1 and 2	12	0.05	0.940
3	curve 1 and 2	12	-0.05	0.940
4	curve 3 and 4	12	0.05	0.940
5	curve 3 and 4	12	-0.05	0.940

FIG. 11. Analysis by the $\phi = 0$ method (example 2).

In all of the foregoing cases, the values of $A_c{}'$ were reasonable.

So far, the assumed side force function $\beta(x)$ covered a large variation. Each time, it eventually reached the bound beyond which the solution became unreasonable. No factor of safety higher than 1.471 or lower than 1.444 was found. The bounds of the factor of safety were therefore determined to be 1.444 and 1.471.

As a check on the program, the $\phi = 0$ method using the same unit weight and a circular failure surface was analysed by a similar integration procedure. The value of the factor of safety in all cases was 0.940 (Fig. 11). This is consistent with the basic principle that, for the $\phi = 0$ method with a circular slip surface, the resulting factor of safety is independent of the assumptions made for the interslice force.

Failure surface 2

Failure surface 2 exits at the toe of a slope. The value of $\beta(x)$ at the left end should be fixed at 31°, which is the inclination of the slope surface at which the slip surface exits (Fig. 6). The original solution gave a value for the factor of safety of 1.682, but is associated with a distribution of F_{ve} that is smaller than unity on the left part due to the relatively high value of $\beta(x)$ in that area (Fig. 12). Curves 3 and 4 were employed to reduce the value of $\beta(x)$ on the left part with a value of ε of 0.025. After 12 integrations, the region lower than the $F_{ve} = 1$ line was reduced appreciably; the factor of safety became 1.639. Although a further effort to make that unreasonable region even smaller is possible, the factor of safety will likely remain around 1.639.

Example 2

Find the value of the factor of safety for the wedge-shaped slide shown in Fig. 13.
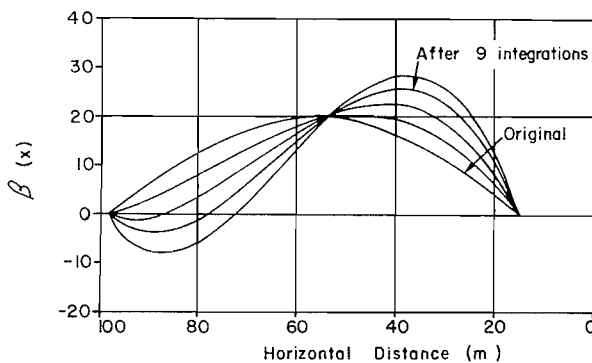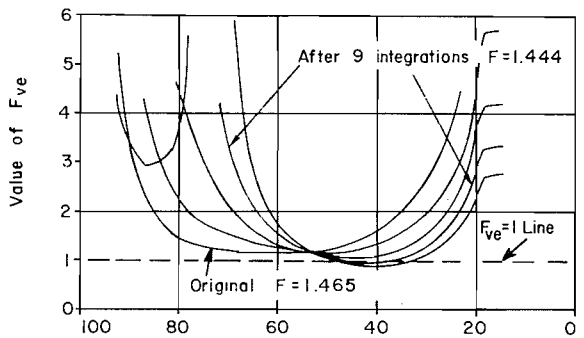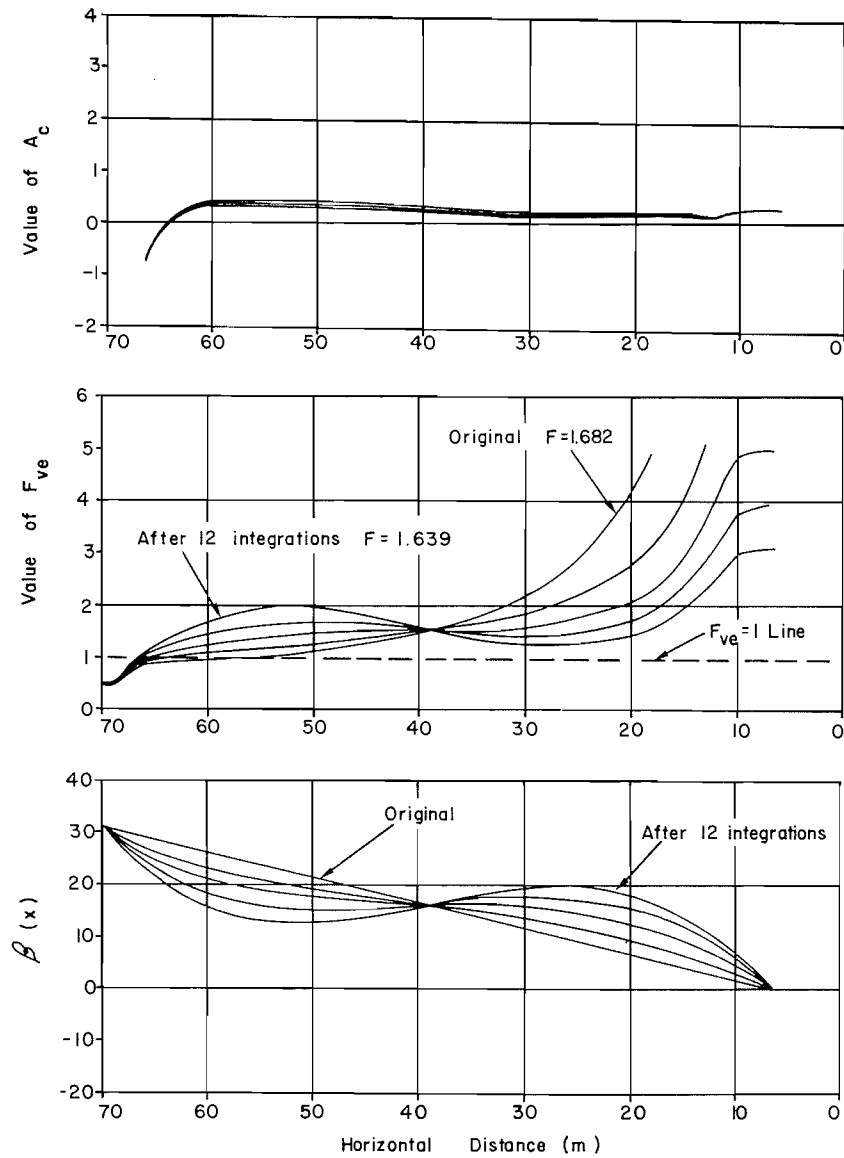
A similar integration procedure is performed for this

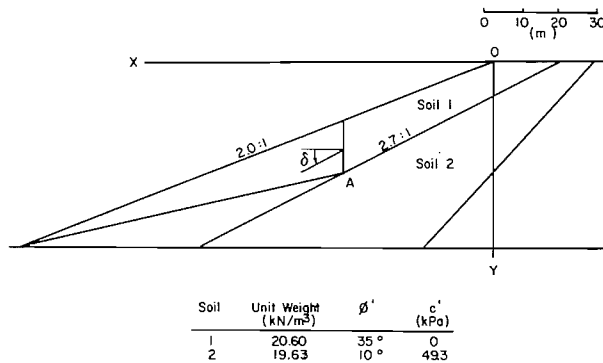FIG. 12. The analysis for failure surface 2 (example 2). Curves 3 and 4 were employed; $\varepsilon = 0.025$.
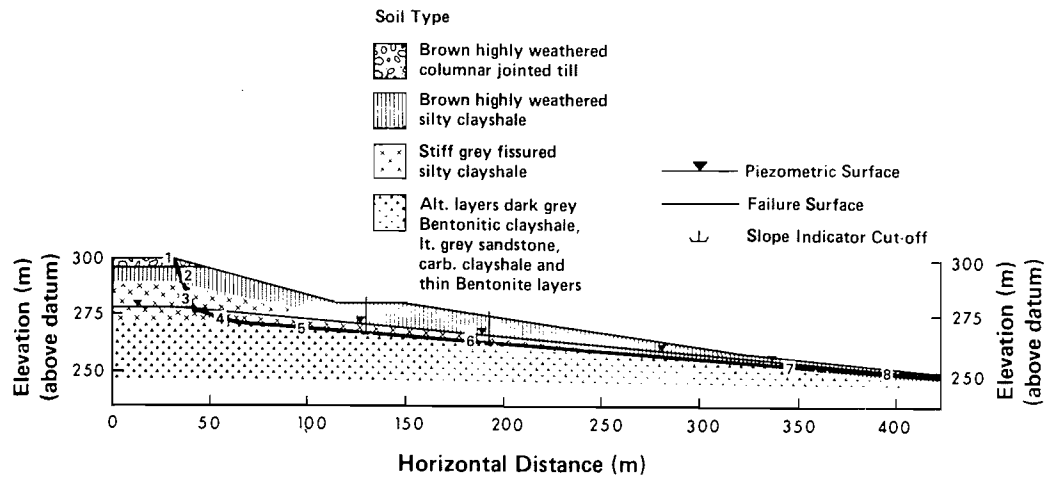

FIG. 13. An example of the wedge slide.

problem. Figure 14 shows the various critical F_{ve} curves that touch the $F_{ve} = 1$ line. The factor of safety ranged between 1.677 and 1.696. It is interesting to note that δ, the value of β at point A at which the inclination of the failure surface changed abruptly, ranged from 17–23°. Near the right end, the value of A_c' is not satisfactory. As was indicated by Spencer (1973), the location of the thrust line is always unreasonable near the crown of a cohesive slope unless a tension crack is considered. Spencer has suggested a method to determine the tension crack associated with reasonable values of A_c' near the crown. A further investigation of the problem in combination with the method developed here would be of interest, but is set aside for further study.
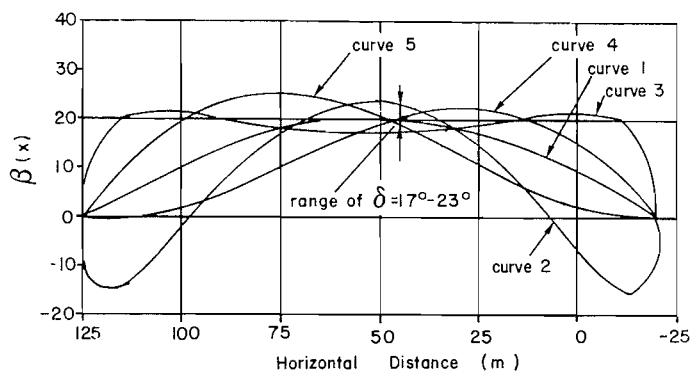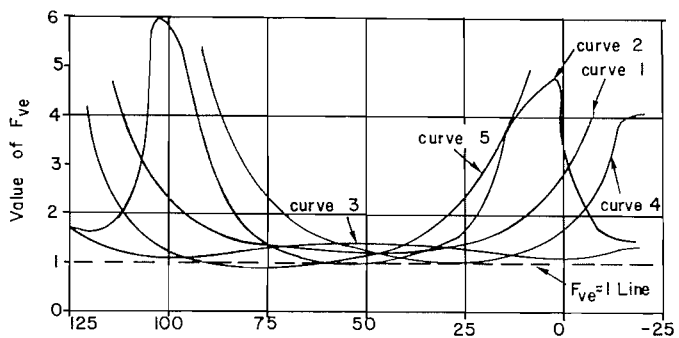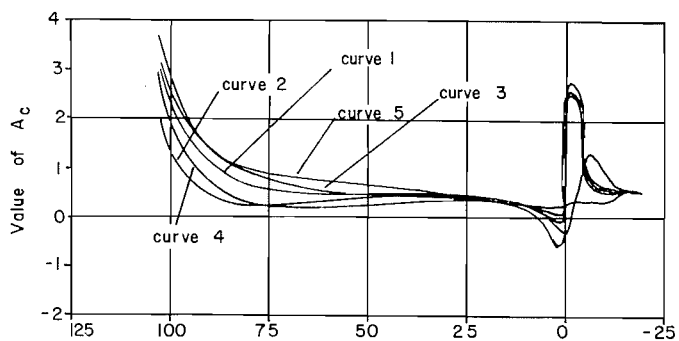
Curve	Integration function	Time of integration	ϵ	F
1	original			1.684
2	1 and 2	6	0.08	1.690
3	1 and 2	3	-0.10	1.680
4	3 and 4	3	0.04	1.696
5	3 and 4	3	-0.04	1.685

FIG. 14. The analysis for the wedge slide (example 2).

FIG. 15. The Edgerton slide (example 3).

Example 3. Analysis of the Edgerton slide (Fig. 15)

The Edgerton slide was analysed by Thomson and Tweedie (1978) and their case 2 is re-analysed here. A factor of safety of 0.958 was found originally. It is interesting to note that in this case the value of A_c' rather than F_{ve} is not satisfactory in the right-hand part of the region (Fig. 16). In order to reduce this unreasonable region, curves 3 and 4 were employed with a value of ε of 0.015. After 9–12 integrations, the values of A_c' over most of the region were reasonable. The corresponding factor of safety is around 0.960.

Conclusions

The generalized method of slices employed in the analysis of slope stability requires that (1) all conditions of equilibrium be satisfied, (2) the Mohr–Coulomb failure criterion be satisfied for a specific definition of the factory of safety, and (3) certain conditions of physical admissibility not be violated.

In addition, an extra assumption must be made to render the problem statically determinate.

It has been shown formally here that the assumptions of the inclinations of the interslice forces or the location of the thrust line are subject to certain restrictions at the ends that have been ignored in previous work. Guidance for satisfying these restrictions are given. A modified iterative procedure has been developed that to date has not encountered the convergence problems that occasionally affect other programs in common use.

The factor of safety in any particular problem is not unique. A procedure has been developed for exploring formally the bounds of the factor of safety within the limits of physical admissibility. It has been shown that, consistent with earlier studies, the variation in the factor of safety when subjected to conditions of physical admissibility is small for all practical purposes. This new analysis confirms the view that variations in the factor of safety between several methods in common use are of little practical significance.
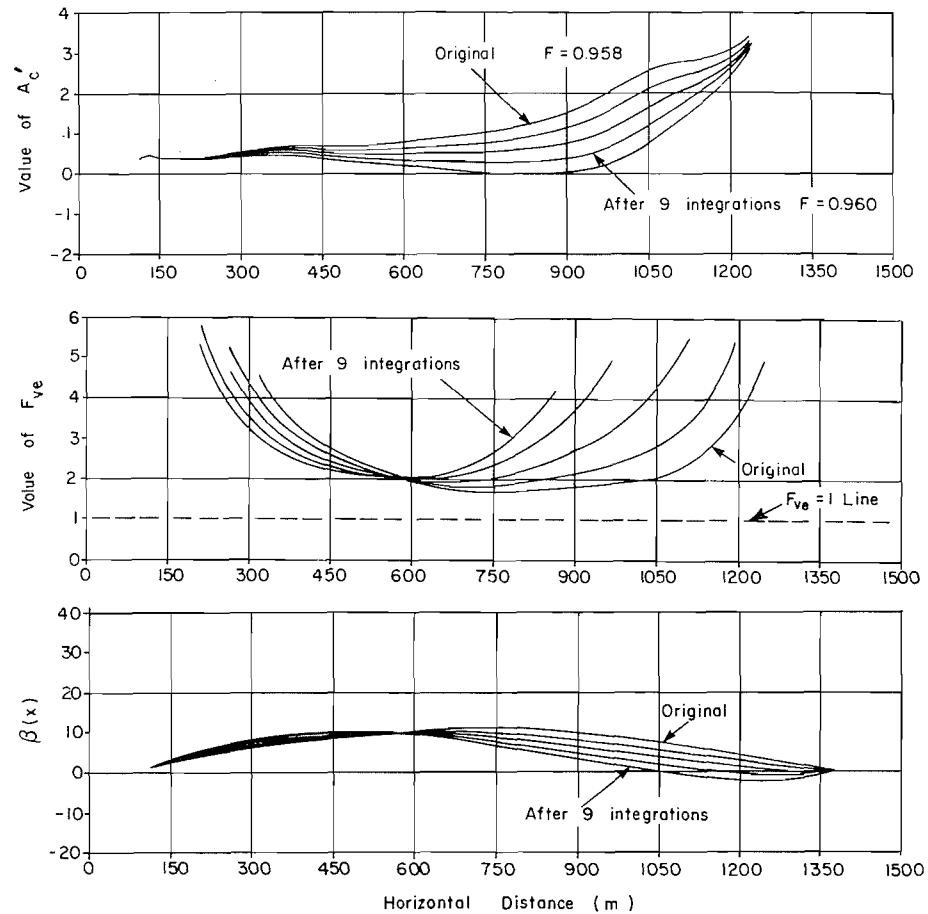
FIG. 16. Search for a reasonable solution (example 3). Curves 3 and 4 were employed; $\varepsilon = 0.015$.

A copy of the new computer program is available from the authors.

Acknowledgements

The authors wish to thank Prof. Y. N. Chen who has carefully investigated and discussed the mathematical deviations. Grateful appreciation is given to Dr. J. Simmons for his helpful discussion of the manuscript and Dr. S. Thomson for his assistance in preparing the material from the Edgerton slide. All the program coding was performed with valuable help from Mr. R. Howells.

BISHOP, A. W. 1955. The use of the slip circle in the stability analysis of slopes. Géotechnique, 5, pp. 7–17.

BISHOP, A. W., and MORGENSTERN, N. R. 1960. Stability coefficients for earth slopes. Géotechnique, 10, pp. 129–150.

CHEN, Z. 1981. On the side force in limit equilibrium analysis of slopes. Internal report, Department of Civil Engineering, University of Alberta, Edmonton, Alta.

JANBU, N. 1954. Application of composite slip surfaces for stability analysis. Proceedings, European Conference on Stability of Earth Slopes, Sweden, 3, pp. 43–49.

———— 1973. Slope stability computations. In Embankment dam engineering. Edited by R. C. Hirschfeld and S. J. Poulos. Wiley, New York, NY, pp. 47–86.

MORGENSTERN, N. R., and PRICE, V.E. 1965. The analysis of the stability of general slip surfaces. Géotechnique, 15, pp. 79–93.

———— 1967. A numerical method for solving the equations of stability of general slip surfaces. Computer Journal, 9, pp. 388–393.

SARMA, S. K. 1973. Stability analysis of embankments and slopes. Géotechnique, 23, pp. 423–433.

SPENCER, E. 1967. A method of analysis of stability of embankments assuming parallel inter-slice forces. Géotechnique, 17, pp. 11–26.

———— 1973. Thrust line criterion in embankment stability analysis. Géotechnique, 23, pp. 85–100.

TAYLOR, D. W. 1948. Fundamentals of soil mechanics. John Wiley and Sons, New York, NY.

THOMSON, S., and TWEEDIE, R. W. 1978. The Edgerton slide. Canadian Geotechnical Journal, 15, pp. 510–521.

WHITMAN, R. V., and BAILEY, W. A. 1967. Use of computers for slope stability analysis. Journal of the Soil Mechanics and Foundations Division, ASCE, 93(SM4), pp. 475–498.